

Contents lists available at ScienceDirect

Spectrochimica Acta Part B: Atomic Spectroscopy

journal homepage: www.elsevier.com/locate/sab





Time-resolved absolute mass of yttrium laser-induced plasma

Jonathan Merten *, Erin Nicholas, Shealyn Chestnut, Shawnda Ethridge, Hannah Bariola, Mary Elizabeth Foster

Arkansas State University, Department of Chemistry and Physics, P.O. Box 419, State University, AR 72467, USA

ARTICLE INFO

Keywords: Laser-induced breakdown spectroscopy Plasma chemistry Laser-ablation atomic absorption spectroscopy Plume-gas interaction Yttrium Absorption spectroscopy Plasma diagnostics

ABSTRACT

The absolute atomized mass of the neutral and first-ion reservoirs of a laser-induced yttrium plasma were measured with high resolution atomic-absorption spectroscopy mapping at various delays and under different noble and oxidizing cover gases. The maximum spatial extent of the plasma was inversely dependent on the molar mass of the cover gas. Time-resolved masses measured under oxidizing atmospheres showed continuous net loss from even the first measured delay (2 μ s). Though their total masses were stable at early delays, plasmas under helium and argon atmospheres also showed net loss of atomized yttrium from an unknown mechanism beyond 4 μ s. The measured total atomized masses during the early stable period under the noble atmospheres were approximately equal (~30 ng) but higher than the masses measured under oxidizing atmospheres.

1. Introduction

In order to achieve quantitation by laser-ablation elemental analysis techniques, either the ablation process must be stoichiometric or the plasma's departure from the sample stoichiometry must be reproduced by matrix-matched calibration. Of course, part of the power of laserablation sampling (including LIBS, laser-induced breakdown spectroscopy- see References [1, 2]) lies in situations where matrix matching is inconvenient or impossible. As such, a deep understanding of the laserablation process and the relationship between sample and plasma stoichiometry is essential, [3] However, the stoichiometry of the laserinduced plasma (LIP) is complex and evolves with time, further complicating any measurement- material leaves the surface as solid particles, liquid droplets, molecules, and atomized (including ionized) species. As the plasma evolves and cools, matter further moves among these reservoirs and potentially to the bulk surface itself (see Reference [4] for a previous spectroscopic investigation of the mass transfer between particle and atomized reservoirs).

The chemical changes in the plasma, particularly the formation of molecules, are under investigation both for their analytical use/implications as well as their potential application to the generation of novel materials. [5–10] This dynamic LIP system is typically studied with emission spectroscopy and crater measurements. The former requires many assumptions and only represents the hotter parts of the plasma and the latter is a grossly static and non-selective picture of an extremely

dynamic process. Historically, the relative content and stoichiometry of a laser-induced plasma (LIP) have been understood dynamically by assuming local thermodynamic equilibrium (LTE) and generating Boltzmann plots of the time-resolved thermal emission signal- effectively calibration-free LIBS (CF-LIBS). [11,12] Such emission measurements are relatively simple and can be time-resolved with modern fast detectors. Of course, it is not possible to measure the ground state in emission, so its relative population is extrapolated from the (Saha-) Boltzmann plot. The extrapolation from upper states (often multiple tens of thousands of wavenumbers above the ground term) back to 0 cm⁻¹ is fraught given the uncertainties in both the emission signal measured in a given experiment and the transition strengths taken from the literature. Furthermore, researchers have previously questioned the validity of the LTE model in understanding the LIP and significant effort has been directed at understanding the impact of potential departures from equilibrium. [13] In any case, LTE-invoking emission diagnostics provide relative quantitation of the plasma absent an (extremely uncommon) absolute calibration of the detector and optical train's response as a function of spectral radiance. [14] Even with such absolute calibration, it is still impossible to quantitate the non-emitting ground and metastable states with passive methods. Ultimately, our goal is to directly measure the extent and stoichiometry of the LIP with temporal and spatial resolution and do so as directly as possible- i.e. without gross assumptions of LTE or homogeneity. Though more complex than the ubiquitous LIBS, laser-ablation atomic absorption spectroscopy (LA-

E-mail address: jmerten@astate.edu (J. Merten).

^{*} Corresponding author.

AAS) may allow a more direct understanding of plasma composition since it can provide spatially resolved measurements of absolute mass. [15]

Merten and Harilal et al. have recently reviewed methods and applications of laser-ablation atomic absorption spectroscopy. [16,17] Despite the growing body of LA-AAS measurements in the literature, most time-resolved LA-AAS measurements employ a single line-of-sight or spatially resolve along a single dimension. As Skrodzki et al. point out, even when LA-AAS measurements account for temporal changes in absorption lineshape, conclusions from such studies are still limited by the fact that the signal from a single line-of-sight convolves changes in the plasma's composition with changes in its (three-dimensional) morphology. [18] Our lab has previously demonstrated the use of laserablation atomic absorption spectroscopy, specifically two-dimensional maps of the line-of-sight- and peak-integrated optical depth, to effectively measure the mass of material in a given state in the entire plasma with nanosecond time resolution. [9,15] Although our previous and current works do assume a degree of LTE, the potential for error is minimized because LA-AAS is able to directly measure the parts of the atomic state distribution function (ASDF) that contain the largest portion of the population, so any partial LTE (pLTE) distribution that they measure is a better representation of the cooled plasma than one measured in emission. For example, consider that 63% of the Y (I) partition function lies below 15,000 cm⁻¹ (the highest energy level probed in the present measurements) even at 8000 K.

In the current work, we use LA-AAS to measure the mass contained in the ground and lower-lying excited levels of the neutral and first ionized state of yttrium and follow the net exchange of mass between these states and other reservoirs. Absorption measurements of yttrium and YO following laser ablation have a substantial history, in part because the element is important to rare-earth superconducting materials. [19-21] Manufacturing these as superconducting films in appropriate form factors is complicated and some schemes include pulsed-laser deposition (PLD). As a result, some of the earliest LA-AAS measurements used yttrium lines as a PLD diagnostic. We have previously measured the evolution of the neutral Ti and V populations in a plasma, but were unable to simultaneously measure the ion populations because the appropriate lines are in the deep UV where we do not have spectral access at present. [9] Yttrium, however, presents a serendipitous combination of moderate richness of both its neutral and first-ionized spectra and Y (I) and Y(II) ground terms that each have multiple transitions in the visible with gf products appropriate for our measurements.

2. Experimental

Figure 1 shows the general arrangement used in the present laserablation experiments. Ablation was on the face of a 5-cm diameter disk (see inset) of yttrium (sputtering target, 99.99%) which was mounted on a rotary stage (ELL18, Thorlabs). The sample was "precleaned" with 5 laser shots at each location prior to each data acquisition, which consisted of 15 subsequent ablations. The sample was rotated between these sets of 5+15 ablations and sanded with 220 grit sandpaper after each full rotation. In order to minimize probe beam obscuration by the sample while simultaneously minimizing eddyinduced asymmetry of the collapsing plasma and attendant mixing, the laser was focused to ablate the face at a position at least ~ 3 mm away from the perimeter of the sample.

Sample ablation was with Nd:YAG fundamental produced by a Big Sky Ultra (Bozeman, MT) operating at 10 Hz (\sim 8 ns). A half-waveplate/polarizer combination was used to attenuate the ablation energy to \sim 16 mJ. The focusing optic (AR-coated f = 15 cm) was operated at its focal length (within 5%). However, the Nd:YAG beam was expanded with a Galilean beam expander in order to increase the effective numerical aperture of the ablation lens and thereby minimize potential for breakdown above the sample and attendant plasma shielding. The beam spot size (0.40 mm) was approximated from the crater diameter, with a

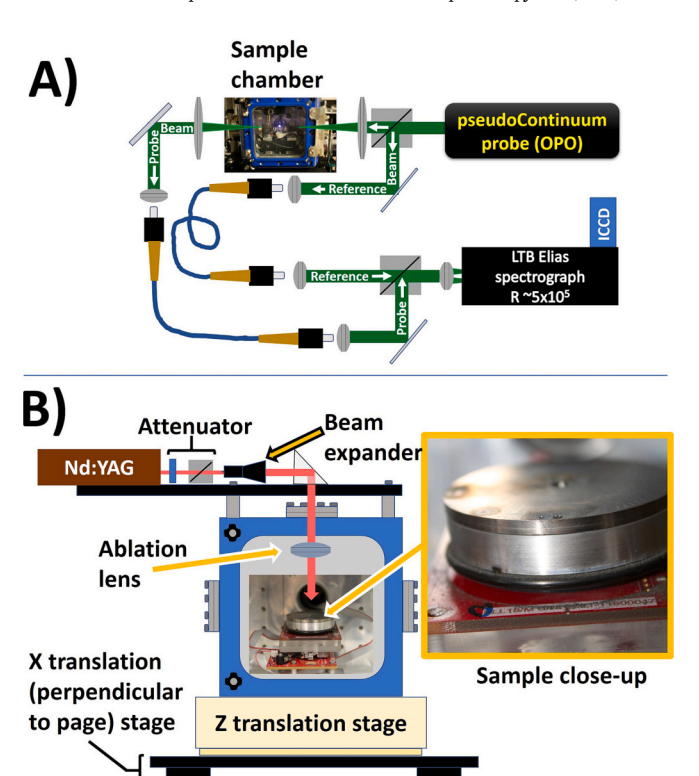


Fig. 1. A) Dual-beam absorption optics and integration with ablation chamber. The dual-beam-in-space arrangement accounts for most of the variable structure of the OPO (see Reference [22]). B) Sample chamber and associated optomechanics used to produce plasma and translate it relative to probe beam (omitted for clarity). The sample and the ablation laser and ablation optics are all contained on a common x-z motion stage. The attenuator consists of a polarizer and a half-wave plate.

resulting fluence of 13 J/cm².

Measurements were made in a vacuum cube at a slightly reduced pressure of 300 mbar as this was found to decrease issues with beamsteering of the probe. The static air, helium (UHP, Airgas), argon (UHP, Airgas), or $80:20~{\rm He:O_2}$ (medical grade, Airgas) atmosphere was monitored with a capacitance manometer. Because of the static atmosphere and because the ablation optic was inside the chamber, the windows and ablation optic were cleaned between images.

Our absorption measurements employed a double-beam-in-space paradigm that we refer to as pseudocontinuum-source atomic absorption spectroscopy (psCS-AAS). We have previously described the technique but provide a description of our updated setup here. [15] The pseudocontinuum is a semicoherent spectral pulse that is broader than the atomic line being measured but narrower than the free spectral range of the echelle spectrograph being used. In this work, the pseudocontinuum was provided by a type II OPO (Model 342A, Ekspla, Vilnius). The pulsed OPO beam was spatially filtered and expanded before being focused at the LIP to generate probe spot sizes from 190 to $280\ \mu m$ as measured with a beam camera. Note that this measured spot size may be somewhat irrelevant since the effective true "spot size" depends on the mutual overlap of the probe focusing optics and the collection optics. Although a smaller spot size at the plasma may have been desirable for improved linearity at high absorbances, $190-280 \ \mu m$ was used as a compromise between linearity of absorbance and the need to avoid kinetic saturation of the transition. [16] The beam was separated into probe and reference arms prior to the sample chamber. Because we have found that standard single-mode fibers lead to distortion of the OPO spectrum through nonlinear effects, probe and reference beams were collected with large-mode-area single-mode photoniccrystal fibers that minimized the potential for nonlinearity. The fiber

outputs were collimated then focused so as to slightly offset the two fibers' images at the entrance slit of an ELIAS I spectrograph (LTB, Berlin). The entrance pinhole of the spectrograph was replaced with a slit by the manufacturer, allowing simultaneous measurement of the probe and reference spectra from each OPO shot on a single ICCD face. The spectrograph was typically operated with singlepassing of the echelle grating, with resolving powers near 5×10^5 reported by the manufacturer, though these are expected to vary somewhat across the spectral range according to the diffraction order used. Dispersion was calibrated at each spectral position with a 6 mm fused silica etalon in the probe beam path.

The interlaser (i.e. ablation-to-probe) delay was controlled with a digital delay generator (DG 645, Stanford Research). In an effort to improve signal to noise ratio (SNR) without excessive ablation, two blank spectral pairs (probe and reference) were recorded for each measurement pair recorded during an ablation. As the lasers are designed to run continuously, the Q-switch triggering channel of the delay generator was controlled with its "inhibit" function so as to only ablate when necessary while still firing the ablation laser flashlamps at 10 Hz to minimize temperature variation in the laser. The inhibit input was driven by an Arduino microcontroller receiving inputs from an S-R digital latch triggered with the arm and fire outputs of the ICCD and a manual reset button. The microcontroller was programmed to produce the 2:1 ratio of blank to ablation measurements. A total of 45 pairs were collected at each spot (30 blank pairs and 15 pairs coincident with plasmas).

The probe beam propagated parallel to the sample surface. The ablation laser, ablation optics and sample chamber were all mounted on a stepper-motor-driven XZ stage. Thus, the relative position of the plasma was translated between acquisitions within the plane perpendicular to the probe beam. Plasma line-of-sight absorptions were recorded on a 300 μm \times 300 μm pitch. Spectra were processed with custom Labview routines to produce absorption spectra (the log₁₀ definition of absorbance is used throughout) that were typically fit to Voigt profiles with OriginPro (Originlab Corporation). When SNR was low, simple Doppler fits were used to avoid overfitting. Integrated absorption peak areas, representing the column depth along a given line-of-sight were converted to masses in the probed lower state assuming a ~ constant column depth at the point spacing. The masses measured at the different lines-of-sight were summed to give the total mass of material in a specific state in the plasma. This procedure also generates a spatial map of the plasma's optical depth and does not assume any particular geometry or symmetry in the plasma. Thus, the measurement does not inherently measure a number density; total mass can be calculated without assumptions about or measurement of plasma geometry.

Our intention is to measure the mass across all of the relevant states with a minimum of assumptions regarding thermal equilibrium. Nonetheless, we do not directly measure states above $\sim 15,000~{\rm cm}^{-1}$ in either the ion or the neutral. Rather, the measured absolute masses in each state were used to construct Boltzmann plots (which notably include a point for the ground term). Absolute masses in a given level were calculated as:

$$\frac{ln(10) \bullet M \bullet \Delta x \bullet \Delta y \bullet \int abs(\lambda) d\lambda}{N_A \bullet \lambda^2 \bullet \int_{lu} \bullet 8.8 \times 10^{-15}} = mass_l \tag{1}$$

where M is the molar mass, Δx and Δy are the measurement spacings in the imaging grid, N_A is Avogadro's constant, λ is the transition wavelength, and \int_{lu} is the transition oscillator strength. Although the considerations surrounding the detection limits of our measurement paradigm are complex and not yet well explored, at late times the masses measured in the most highly excited level are less than five picograms in a given plasma mapping (individual lines-of-sight presumably interact with substantially less than this). With the assumption of LTE, the partition function (Z(T)) and y-intercept (b), the Boltzmann plots are effectively extrapolated to the ionization limit, calculating the total mass

in a given ionization state using:

$$mass_t = Z(T) \bullet e^b$$
 (2)

Although we would like to avoid assumption of LTE, measuring every term in the ASDF would be unreasonably tedious. While we do invoke LTE out of this necessity, our Boltzmann-plot extrapolation is to the less-occupied extreme of the ASDF so the error created by the extrapolation is reduced relative to Boltzmann plots in emission. Transition information and partition functions were taken from the NIST database and references therein and is summarized in Table 1. [23–25]

The Y(I) ground-term absorptions measured at 622.258 nm exceeded the linear dynamic range of our measurement in many cases (and led to measurement conditions wherein the requirements of Beer's Law are not well met, as discussed in [16]) and we were forced to use the weaker 658.486-nm transition, for which an oscillator strength is not reported. To transfer the calibration to this unknown line, plasma optical depth measurements were taken under conditions allowing serial measurement of both the unknown and a calibrated transition without saturation (i.e. an alloy containing 20% yttrium was ablated at a reduced pressure in order to keep the highest absorbance below $\log_{10}(I_0/I) = 1.5$). We note that similar "transfer" of calibration by LA-AAS has been demonstrated for gadolinium recently. [26] Unfortunately, our setup is not capable of measuring multiple transitions simultaneously along a single line-of-sight, so the different transitions were measured serially over several hours.

Measurements to the red of 600 nm are particularly difficult for our setup because of the combination of low and broadened optical parametric generation at the red edge of the type II curve and the low efficiency of the detector and spectrograph as we approach the near infrared, where there are gaps in the single-pass spectral coverage of the spectrograph. Because the more convenient 640.201-nm transition was only accessible with our spectrograph in double-pass and because the ratio of the gf products of the 640.201-nm to 658.486-nm transition was nearly 14 (straining our linear dynamic range), the calibration transfer was effected in two steps: 622.258 nm to 655.737 nm, then 655.737 nm to 658.486 nm. Because the 655.737-nm and 658.486-nm transitions originate in lower levels of different energies, a correction was required to account for the expected ratio of the two different energies (a factor of ~0.87 near 5500 K, assuming Boltzmann statistics). To this end, absorption was measured at the 443.734-nm transition, then combined with the 655.737-nm absorption to determine the temperature (and thus, the expected ratio of the ground and 530.51-cm⁻¹ levels). The modest separation of the ground-term levels that we are calibrating between should minimize the potential impact of any error in the Boltzmann temperature on our determination of the oscillator strength. After repeated measurements of the oscillator strength, the standard error our experiment was minor at 3% in comparison to the 18% due to the uncertainty in the literature value, which appears to stem from the branching ratio. [24] See Reference [27] for discussion of the techniques for and difficulties in measuring oscillator strengths.

Table 1- transitions used. Oscillator strengths were taken from Reference [23] except for starred (*) values, which were calibrated as described in the text.

| Species | E _{lower} (cm ⁻¹) | glower | Oscillator strength | Wavelength (nm) | Uncertainty |
|---------|--|--------|------------------------|--------------------|-------------|
| Y(I) | 530.51 | 6 | 2.52×10^{-4} | 658.486 | 18% * |
| Y(I) | 530.51 | 6 | 1.10×10^{-3} | 640.201 | 18% |
| Y(I) | 0.00 | 4 | $1.63 	imes 10^{-3}$ | 655.737 | 18% * |
| Y(I) | 0.00 | 4 | $5.1 	imes 10^{-3}$ | 622.258 | 18% |
| Y(I) | 11,078.61 | 6 | 2.54×10^{-2} | 443.734 | 6% |
| Y(I) | 14,948.99 | 4 | 4.7×10^{-2} | 549.315 | 25% |
| Y(II) | 840.20 | 3 | 2.36×10^{-3} | 419.927 | 4% |
| Y(II) | 3296.18 | 5 | 6.20×10^{-3} | 468.232 | 3% |
| Y(II) | 8003.13 | 5 | 8.60×10^{-3} | 511.911 | 9% |
| Y(II) | 14,018.27 | 5 | 1.59×10^{-2} | 554.601 | 11% |

3. Results and discussion

Line-of-sight maps for the neutral's ground term are given in Fig. 2. As we demonstrated with our earlier titanium data (Reference [9]), the plasma is more confined under He:O2 relative to plasmas under pure helium, but maintains a grossly similar morphology at early times, then rapidly shrinks. Air leads to an even more confined plasma in the present vttrium data as might be expected from the progression of molar masses. The yttrium morphologies under argon are unique in that the plasma's distal cap appears completely separated from the cloud at the sample surface, then slowly "reconnects" as the distal mass expands and the base disappears. Splitting of the plasma under different atmospheres has been modeled by Wood et al. but their measurements and models were developed for pulsed laser deposition conditions, with pressures at least two orders of magnitude lower than the 300 mbar of our recent studies. [28] Aguilera et al., on the other hand, have made meticulous Abelinverted emission measurements of relative Fe(I) and Fe(II) populations 3 µs after ablation under air. [29] Their measurements show a cap of neutral material somewhat similar to the 2 µs point under air in our Fig. 2. Unlike their measurements, which show no material at the sample surface (see both References [29,30]), we see substantial material at the surface under certain conditions (see Fig. 2). This could be due to different ablation conditions and subsequent hydrodynamics, though we suggest that it stems from our different measurement paradigm, which does not "weight" its representation to the hotter parts of the plasma. In previous measurements of titanium neutral, our group has observed a maximum in ground-state neutral absorption in the loweremissivity region at the sample surface. [15] While the previous Ti ground-state morphologies had substantial mass at the surface, they lacked the distal caps seen in the present yttrium data, presumably because of a combination of different focusing (i.e. larger spot size), different energy (25 mJ) and a higher pressure of helium cover (1 atm) with resultant differences in the plume hydrodynamics.

In interpreting all of our data, including Boltzmann-plot-derived quantities, it must be remembered that the measurements are made in absorption rather than the emission measurements normally encountered in the literature. Furthermore, since each point in the Boltzmann plot is the total degeneracy-normalized mass measured across the whole plasma for a given level, there is inherent spatial averaging. Boltzmannderived excitation temperatures are given in Fig. 3 and Fig. 4. Because of the relatively high uncertainties in the literature oscillator strengths for the ground-term neutral (and therefore the results of the calibration transfer- see Table 1), we calculated the uncertainties in Boltzmann plotderived quantities with two different sets of assumptions: 1) assuming that random error in our measurements dominated (i.e. propagating uncertainty from the standard error of the calibration slope) and 2) assuming that uncorrelated error in the literature oscillator strengths dominated. To generate the uncertainties for the second assumption case, a Monte Carlo simulation incorporating the (assumed independent) uncertainties in literature oscillator strengths was coded in Labview. The simulation accounts for the partition function's dependence on temperature and thereby produces distributions of both temperature and total mass.

The error bars in Fig. 3 use assumption case 1 (i.e. dominance of random error in our experiments). In general, the ion data are likely well-represented by case 1 because of the relatively low uncertainties in their oscillator strengths. The reported 18% uncertainty in the ground-term oscillator strength used for the neutral (see Table 1) is quite large and one must also consider the potential for systematic error due to the tabulated oscillator strengths (error assumption case 2). Fig. 4 compares temperatures calculated under He and He/O2 using error assumption cases 1 and 2. Since the case 2 error should be mostly systematic (i.e. correlating), comparison between atmospheres in our data is reasonable in Fig. 3 (thus our use of assumption case 1 in Fig. 3). In any case, the small uncertainties from assumption case 1 highlight the precision of our absorption technique when oscillator strengths are well

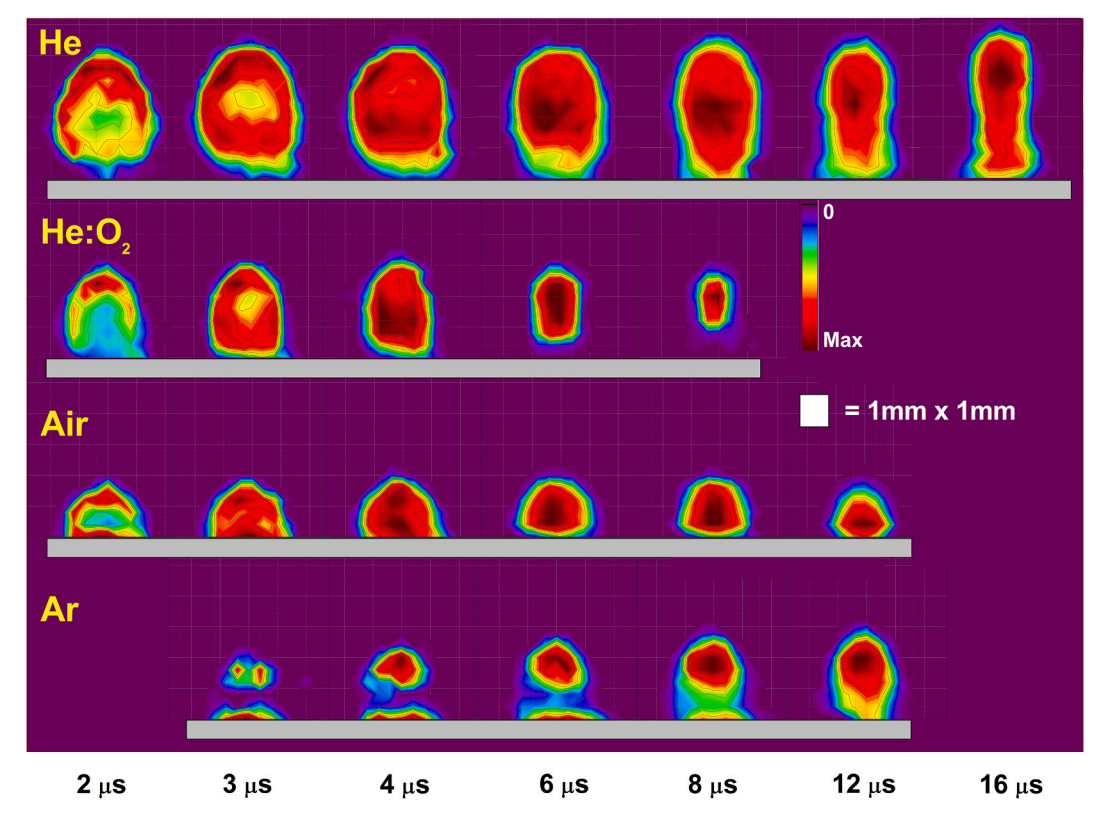


Fig. 2. Line-of-sight absorption maps for the ground term of the neutral. The 658.486-nm and 655.737-nm lines were used for the noble and oxidizing atmospheres, respectively. The ablation laser is incident from above and the grey bars indicate the sample surface. Note that each image is individually color-scaled to emphasize morphology and that the spatial scale is slightly anisometric.

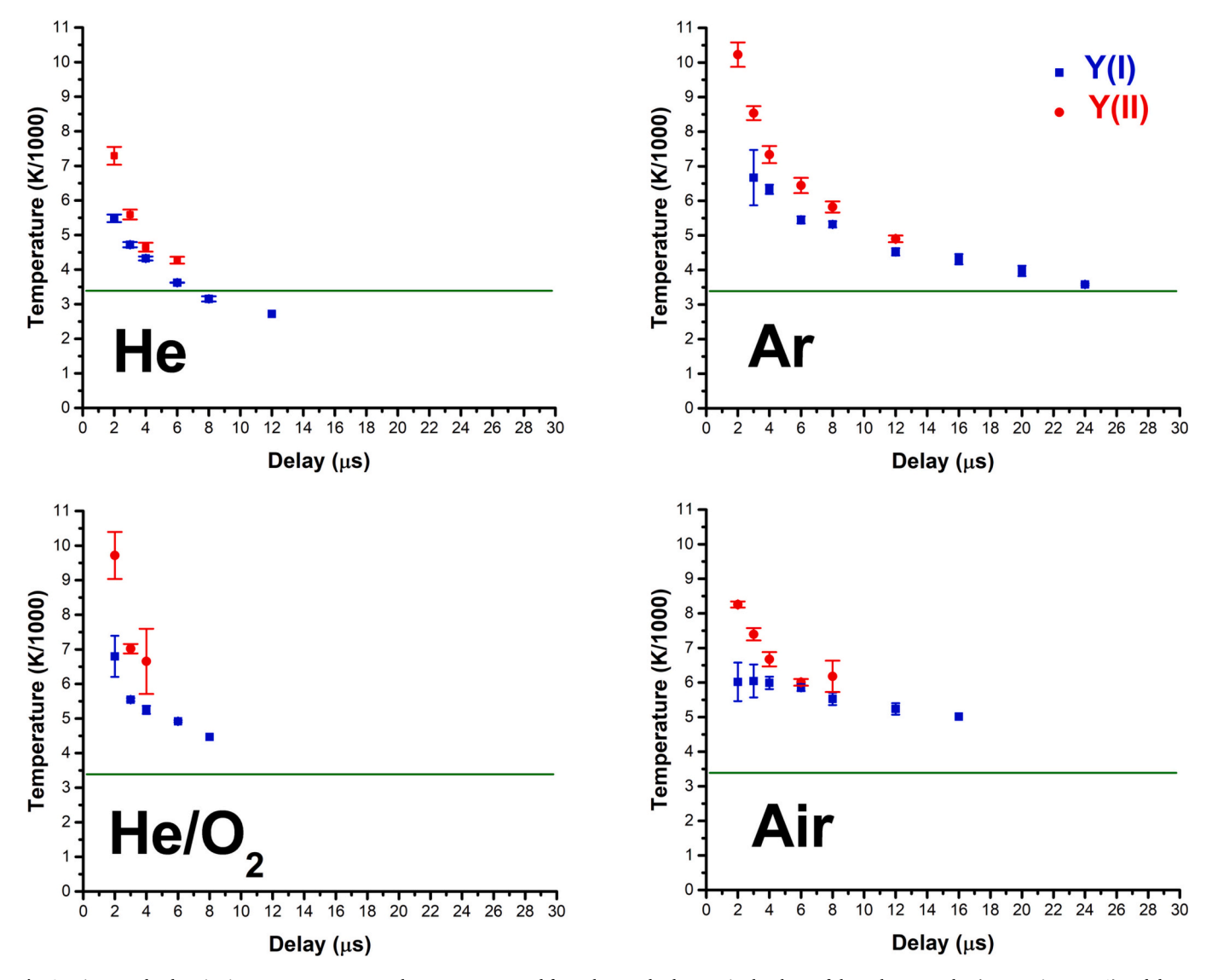


Fig. 3. Time-resolved excitation temperatures. Error bars are propagated from the standard errors in the slope of the Boltzmann plot (assumption case 1) and do not account for the uncertainty in the oscillator strengths. The green line is the boiling point of yttrium at 300 mbar. Note that it was not possible to measure the 2-μs point for Y(I) under argon. (For interpretation of the references to color in this figure legend, the reader is referred to the web version of this article.)

known.

As is generally expected from its high thermal conductivity and is established in the literature with emission measurements (see, e.g. References [31, 32]), the excitation temperatures under helium are lower than under the other gases. Temperatures under argon are highest, but approach those under air at longer times. Under helium the neutral temperatures appear to drop below the boiling point (3300K) of yttrium at this pressure by 8 µs. Presumably, cooling below the pure metal's boiling point indicates dilution in the cover gas rather than any supercooling or measurement error. We have previously observed (with absorption measurements) neutral temperatures below the boiling point when ablating a titanium alloy under helium with the same setup. [9] Kautz et al. have observed uranium excitation temperatures (under atmospheric-pressure air) well below the boiling point with thermal emission measurements. [7] However, in our data with oxidizing atmospheres, the yttrium absorption signal becomes too faint for us to measure before the vapor temperature drops below the boiling point.

In general, the ion temperatures are significantly higher than the neutral temperatures (this observation is subject to our systematic error but is generally expected). This is likely because of inhomogeneity in the plasma- i.e. the hotter regions of the plasma are more ionized, while the

neutrals represent the cooler regions, as discussed by Aguilera and Aragon. [29] Fig. 5 demonstrate the complementary distributions of the neutral's ground term and a highly excited ionic level under the two noble atmospheres. The existence and significance of this inhomogeneity has been previously demonstrated in emission measurements by other authors (e.g. Reference [29]). The ion densities in our data are substantially more removed from the sample surface than those of Reference [29]. Given the difference in ablation energy and the fact that we operated at 1/3 the pressure of their data, such differences are easily attributed to slight differences in hydrodynamics. Radially, our morphology data (Figs. 2 and 5) are similar to those of Aragon et al.- the ion absorption is more central while the neutral absorption is more peripheral. [30] It should be noted that their data are presented after Abel-inversion (in contrast to our line-of-sight measurements), making the comparison to ours less than intuitive. Generally, morphological and thermal inhomogeneity would be expected to disappear (as seen in Fig. 2) as gradients flatten with time due to diffusion and turbulent mixing.

The extracted neutral and first-ion masses are given in Fig. 6. For simplicity, we only show the standard-error-propagated uncertainties (i. e. the assumption case 1 above). Once again, the case 2 uncertainties

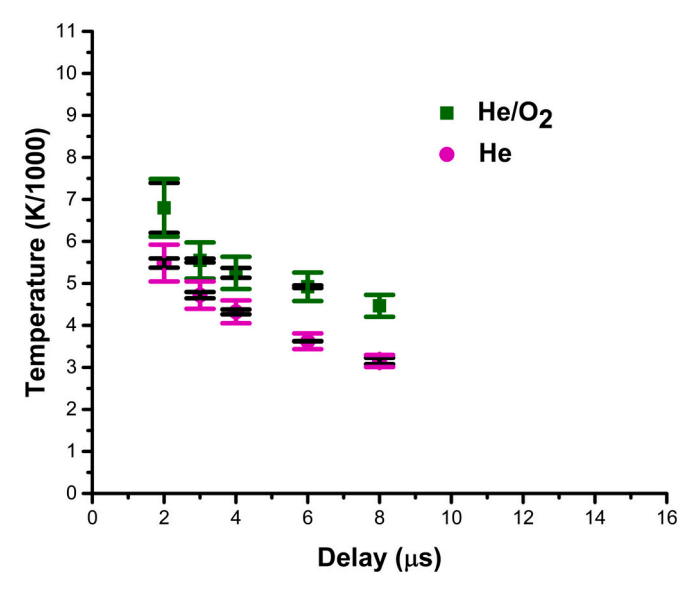


Fig. 4. Comparison of Y(I) temperatures and error propagation methods under He and He/O_2 . The black error bars are propagated uncertainties (assumption 1) and the colored error bars are the Monte-Carlo-simulated error which take into account uncertainties in oscillator strength (assumption 2).

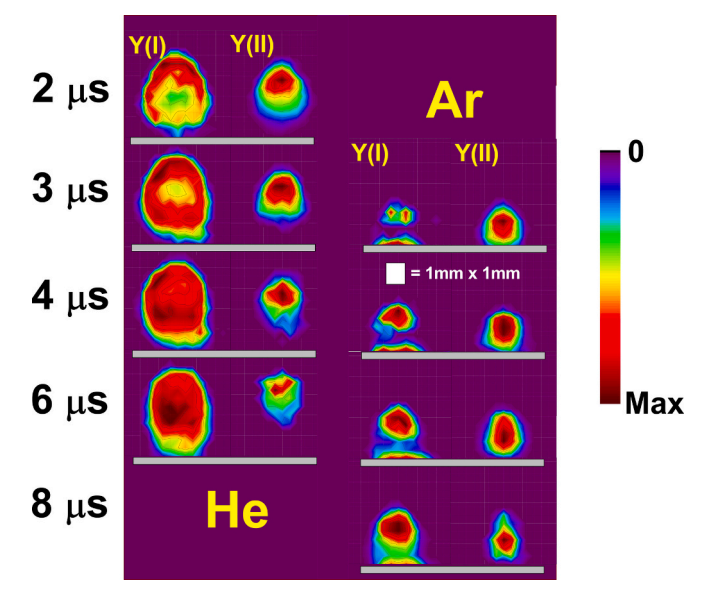


Fig. 5. Morphologies measured with Y(I) ground term (658.4855-nm transition) and an excited (14,018 cm $^{-1}$) level of Y(II) under the two noble atmospheres. Note that each plasma image is individually color-scaled to emphasize morphology. The ablation laser is incident from above and the grey bars indicate the sample surface.

(Monte Carlo estimations derived from uncertainties in literature oscillator strengths) would tend to correlate across delays (read: evolving ASDF's) and between cover gases. As such and to minimize clutter in the figure, the significance of the case 2 error assumptions in mass measurements is considered later.

In all cases, the mass data show that the plasmas are still mostly ionized at our earliest data points. As would be expected, the exchange between ion and neutral states is fastest in helium, where the observed neutral mass peaks around 7 μ s. The maximum observed neutral mass is only slightly later under argon (\sim 9 μ s). On the other hand, the neutral content of the plasmas in oxidizing atmospheres peaks much earlier (3 and 4 μ s under He:O₂ and air, respectively) and is much lower. We

observed a similar trend in the neutral titanium and vanadium data in our previous work. [9]

With the present yttrium measurements, we hoped to observe a definitive "total ablated mass" under all of the atmospheres by combining Y(II) and Y(I) masses. Their sum in Fig. 6 shows clear and rapid loss of the total mass under the oxidizing atmosphere, with halflives of 3–5 µs. The two-state totals under the oxidizing atmospheres did not show plateaus at any delay and were mutually similar (within uncertainty) at 2 µs. Although we were unable to measure the neutral content at $2 \mu s$ under argon, the trend indicates that it should be close to zero with the total mass thus equal to the ion mass. As such, the argon data appear to show a plateau (in contrast with the oxidizing atmospheres) in combined mass from 2 to 4 µs, beyond which the mass decreases to a second plateau consisting only of neutrals. Similarly, the total mass under helium is constant to within a few percent from 2 to 4 μs. This initial plateau is very slightly higher in mass under helium, recalling argon's greater tendency to produce plasma shielding during ablation (see, e.g. Reference [33]).

At 2 µs measured totals under He/O₂ and air are approximately 18 ng, while the totals under the noble gases are over 50% higher. It is unclear if this is because a similar mass is ablated and atomized in the presence of oxygen but has already begun to react away by 2 µs or if it is the result of modification of the laser-cleaned surface by oxygen between shots, or perhaps because a different mass is ablated (e.g. because of increased plasma shielding). Intershot surface reactions could be important if we assume that the surface remains chemically clean between shots under the noble gases, while the oxidizing atmosphere results in rapid (intershot) chemical modification of the surface such that every shot ablates an oxide-modified surface, with its modified stoichiometry and reflectivity, etc. Assuming a (pure, unoxidized) bulk yttrium density of 4.5 g/cm³ and a crater diameter of 0.4 mm, the 30 ng of material from Fig. 6 implies removal of ~50 nm of material per pulse. It seems unlikely that an oxide layer of tens of nanometers forms in the 100 milliseconds between shots. Thus, we suggest that a similar amount of yttrium is ablated under the oxidizing atmospheres but has already begun to form a significant fraction of YO and higher oxides by 2 μs and note that Diaz and Hahn have reported evidence of plume-plasma chemistry within 200 ns when ablating graphite under air. [34] They also report that the emission persistence decreased as Ar > air \sim N₂ > He. Given that air and nitrogen are reactive, this indicates that their decreased cooling (which affects both chemical and electronic excitation equilibria) and/or increased confinement potential relative to helium is more important than their potential to react. Merten et al. compared persistence of copper emission in aluminum microplasmas under helium and air and found that the signal initially decreased faster in air but that the rates became comparable at 125 ns (the timescale of evolution is faster in such microplasmas). [35] In our present absorption data, the yttrium mass disappears faster under He:O2 than under air, presumably because the faster cooling (see Fig. 3) under He:O2 results in a faster shift in the metal/metal-oxide equilibrium.

The above discussion of total masses neglects the uncertainty due to potential error in the tabulated oscillator strengths of the neutrals. In particular the relatively poorly known oscillator strengths for the ground term of the neutral may prevent useful conclusions about the evolution of the total mass. The Monte Carlo simulations showed the uncertainties in neutral mass to be substantially higher than the uncertainty from our measurement error. Fig. 7 replots the neutral and total masses for plus and minus one (Monte Carlo) standard deviation of error in neutral mass along with the original ion and neutral data. We ignore the impact of the ion's oscillator strength uncertainties since these are better known. Furthermore, we do not plot the assumption case 2 uncertainties as the usual error bars since this error should largely correlate from one time to another and between gases. In either extreme for the case 2 errors, it seems that there is a plateau or near-plateau of total mass between 2 and 4 µs that might provide a quality estimate of the material removed under the noble atmospheres. The durability of

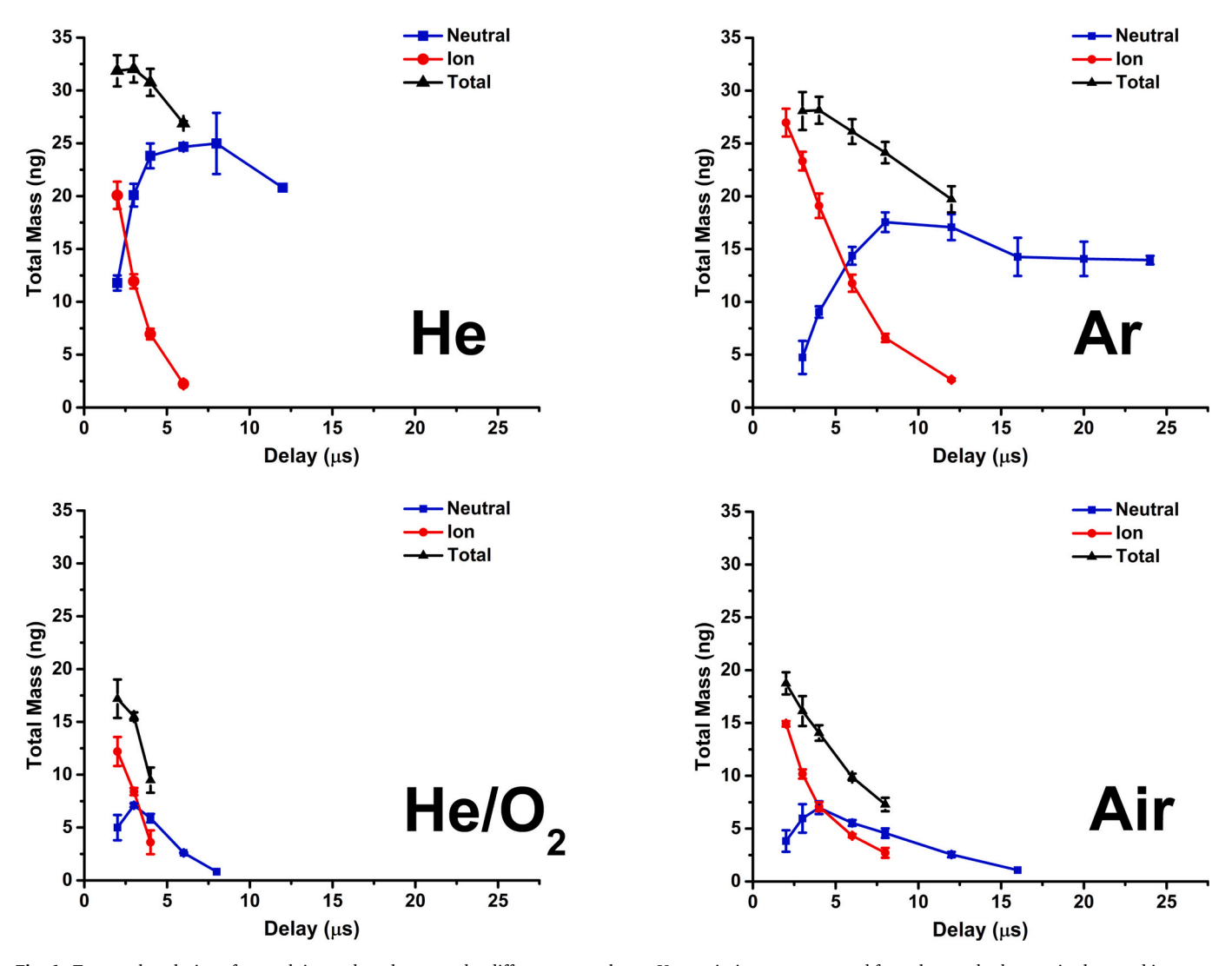


Fig. 6. Temporal evolution of neutral, ion and total mass under different atmospheres. Uncertainties are propagated from the standard errors in slope and intercept.

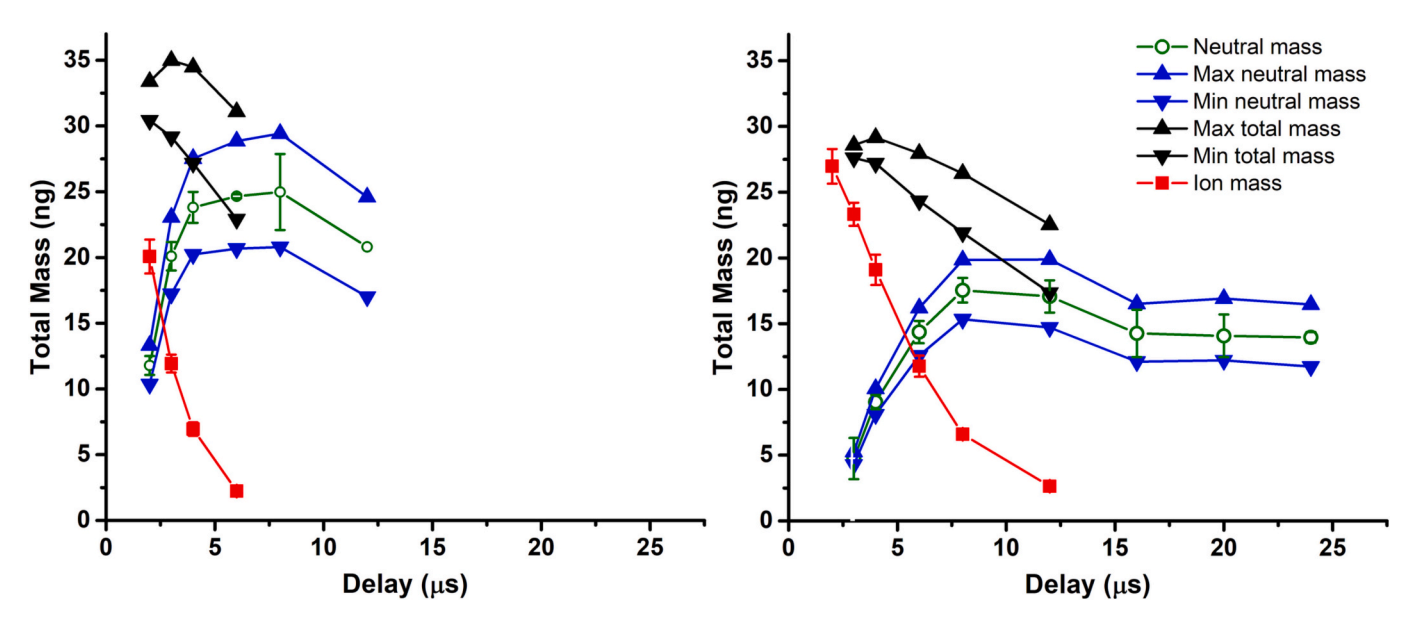


Fig. 7. Masses for limiting cases of error in the calculated neutral and total masses under noble gases (L- He, R-Ar). The two cases correspond to plus and minus one standard deviation in the Monte Carlo simulation (i.e. potential systematic error) at each delay. Where provided, error bars are simple propagated (random) uncertainties for comparison with Monte Carlo uncertainties.

this conclusion stems mostly from the plateau's location at the early times where most of the mass is ionized, rendering the uncertainty in the neutral mass less relevant. Under either noble atmosphere, the peak in *neutral* mass is substantially less than the (earlier) plateau/peak in *total* mass. As such, the neutral mass alone would be a poor estimator for total ablated mass even after the ionization fraction becomes insignificant.

For the sake of completeness, we must acknowledge that any maximum in the measured mass does not strictly prove that there is no gain or loss of mass from either of the summed ion + neutral masses; it only means that there is no net change in their sum at such times. For example, losses from the Y(I) + Y(II) states at early times could be offset by recombination of Y(III). However, we view this as unlikely given Saha-Boltzmann values at the temperatures measured here. Consider, for example, that Gaft et al. observed doubly ionized material only during the first few hundred nanoseconds of plasma evolution in a study of iron and boron. [36] As such, the Y(III) has likely recombined before our first data point. Alternatively, there could be continued evaporation of particles/droplets into the plasma or dissociation of molecules and clusters in some parts of the plasma compensating for losses of atomized yttrium in other regions of the plasma. Although their study employed droplets, Diwakar et al. observed that the flux of bulk material from a particle and into their LIP resulted in perturbation well beyond 10 us. [4] Thus, particles might be a more reasonable confounding factor in our

Irrespective of the potential for systematic error or confounding effects, we do observe a net loss of atomized material by $\sim 6~\mu s$ under all of the atmospheres. Under the O_2 -containing atmospheres, this net loss (see Fig. 6) is presumably the result of oxidation. The route of the loss of mass under the noble atmospheres after 4 μs is less clear. Although our previous work with titanium and vanadium only measured the neutral, there was clear loss beyond $\sim 7~\mu s$ when using a static noble atmosphere, yet there was no evidence of thermal emission from TiO formed due to residual oxygen. On the other hand, Rhoades et al. observed CeO (by absorption spectroscopy) even when ablating the pure metal under 50 Torr of nominally pure nitrogen. [37]

In any case, the current combined Y(I) and Y(II) measurements give a more complete picture of the dynamic stoichiometry in the plasma because recombination of the Y(II) no longer masks any neutral losses at early times. We speculate that these losses could be due to deposition as particles, formation of dimers and higher molecules, oxidation by residual oxygen, or outward diffusion to regions where net signal is below the limit of detection, among other possibilities. However, we note the appearance of several small and closely spaced absorption lines near the 468.232-nm Y(II) line at longer times even under noble atmospheres (data not shown). These do not match yttrium atomic lines. As these lines are particularly intense under the oxidizing atmospheres and the YO blue system occurs in this vicinity (see Reference [8]), we believe that we are observing YO in absorption and that it is at least partially responsible for the late losses observed under the noble atmospheres. It should be noted that the YO bond energy is relatively high (7.4 eV), so the oxide bond would be relatively favored even at high temperatures when oxygen is available. [38]

4. Conclusions

We have transferred oscillator strength calibration to a weak and previously uncalibrated line of the ground term of neutral yttrium. This has allowed measurement of the absolute neutral and ionic mass embodied by a yttrium LIP as a function of time using absorption spectroscopy. The oxygen-containing atmospheres show substantial and early net loss of the atomized material, presenting substantially less atomized material than noble atmospheres even as early as 2 μs . However, even the noble atmospheres show the beginning of net loss of atomized material after 4 μs . This indicates that any attempts to measure the "ablated mass" will require measurement of both ion and neutral lines at an early time.

In the future, we will extend these measurements to different ablation conditions to check if this conclusion is robust or specific to the current experimental conditions (cover gas, analyte, matrix, fluence, energy, etc.). Furthermore, we are working to add an ultraviolet pseudocontinuum probe to our experiment to give access to first-ion lines of other metals- e.g. iron, for which the metal-oxide bond energy is less than yttrium (4.2 vs. 7.4 eV), which should make the experiment less sensitive to residual oxygen. [38] Unfortunately, ion line oscillator strengths tend to be (relatively) poorly known when they are known at all, which complicates identification of other suitable analyte systems for these measurements.

Our current comparison of the air and noble data demonstrates the importance of oxidation (and chemistry, more broadly) to the plasma composition, with substantially longer atom/ion persistence under the noble gases. The oxygen-linked losses of atomized mass under the reactive atmospheres appear within the temporal window used for LIBS analytical measurements. As such, the loss of atomized analyte (and the appearance of emission from molecules formed by oxidation of matrix atoms under air) within the analytical measurement delay window may be responsible for the fact that LIBS detection limits are substantially lower under noble gases.

Multiple LA-AAS studies in our laboratory and elsewhere have shown that oxidation proceeds differently for different metals in the plasma. [9,19] In the current study, the chemical reactions resulted from the mixing of atmospheric oxygen with the sample plume. Presumably, the impact of sample-derived oxidizers is similar or greater since mixing is unnecessary when the chemistry is between sample components. As a result, we are working to identify a suitable system to study the impact of *matrix* chemistry and stoichiometry on the evolution and persistence of the LIP's atomized vapor. We hope to use the combination of ion and neutral masses to study the dynamics of plasma stoichiometry for different elements to better understand chemical reactions' influence on LIBS calibration and matrix-matching, as well as any influence on the formation of particles in the cooling and reacting plasma.

Author statement

Jonathan Merten- funding, experiment design, data processing, manuscript preparation.

Erin Nicholas- data collection and processing. Shawnda Ethridge- data collection and processing. Hannah Bariola- data collection and processing. Shealyn Chestnut- data collection and processing. Mary Foster- data collection and processing.

Declaration of Competing Interest

No.

Data availability

Data will be made available on request.

Acknowledgements

This work was supported by NSF award number 1905301.

References

- J.P. Singh, S.N. Thakur, Laser-Induced Breakdown Spectroscopy, Elsevier, Amsterdam, 2007, p. 429.
- [2] A.W. Miziolek, V. Palleschi, I. Schecter, Laser-Induced Breakdown Spectroscopy (LIBS), Cambridge University Press, Cambridge, 2006.
- [3] R.E. Russo, X. Mao, J.J. Gonzalez, V. Zorba, J. Yoo, Laser ablation in analytical chemistry, Anal. Chem. 85 (2013) 6162–6177.
- [4] P.K. Diwakar, S. Groh, K. Niemax, D.W. Hahn, Study of analyte dissociation and diffusion in laser-induced plasmas: implications for laser-induced breakdown spectroscopy, J. Anal. At. Spectrom. 25 (2010) 1921–1930.

- [5] I.B. Gornushkin, V.P. Veiko, Y.Y. Karlagina, A.A. Samokhvalov, D.S. Polyakov, Equilibrium model of titanium laser induced plasma in air with reverse deposition of titanium oxides, Spectrochim. Acta B At. Spectrosc. 193 (2022), 106449.
- [6] A.A. Bol'shakov, X. Mao, J.J. González, R.E. Russo, Laser ablation molecular isotopic spectrometry (LAMIS): current state of the art, J. Anal. At. Spectrom. 31 (2016) 119–134.
- [7] E.J. Kautz, M.C. Phillips, S.S. Harilal, Unraveling Spatio-temporal chemistry evolution in laser ablation plumes and its relation to initial plasma conditions, Anal. Chem. 92 (2020) 13839–13846.
- [8] M. Gaft, L. Nagli, I. Gornushkin, Y. Raichlin, Review on recent advances in analytical applications of molecular emission and modelling, Spectrochim. Acta B At. Spectrosc. 173 (2020), 105989.
- [9] J. Merten, E. Nicholas, S. Ethridge, H. Bariola, S. Chestnut, A. Anders, J. Brees, M. Foster, Following laser-induced plasma stoichiometry with atomic absorption spectroscopy, Spectrochim. Acta B At. Spectrosc. 200 (2023), 106600.
- [10] C.G. Parigger, Atomic and molecular emissions in laser-induced breakdown spectroscopy, Spectrochim. Acta B At. Spectrosc. 79 (2013) 4–16.
- [11] A. Ciucci, M. Corsi, V. Palleschi, S. Rastelli, A. Salvetti, E. Tognoni, New procedure for quantitative elemental analysis by laser-induced plasma spectroscopy, Appl. Spectrosc. 53 (1999) 960–964.
- [12] J. Hermann, C. Gerhard, M. Burger, V. Craciun, F. Pelascini, Progress in calibration-free laser-induced breakdown spectroscopy, Spectrochim. Acta B At. Spectrosc. 200 (2023), 106595.
- [13] G. Cristoforetti, A. De Giacomo, M. Dell'Aglio, S. Legnaioli, E. Tognoni, V. Palleschi, N. Omenetto, Local thermodynamic equilibrium in laser-induced breakdown spectroscopy: beyond the McWhirter criterion, Spectrochim. Acta B At. Spectrosc. 65 (2010) 86–95.
- [14] D.W. Hahn, N. Omenetto, Laser-induced breakdown spectroscopy (LIBS), part I: review of basic diagnostics and plasma-particle interactions: still-challenging issues within the analytical plasma community, Appl. Spectrosc. 64 (2010) 335A-366A.
- [15] J. Merten, B. Johnson, Massing a laser-induced plasma with atomic absorption spectroscopy, Spectrochim. Acta B At. Spectrosc. 149 (2018) 124–131.
- [16] J. Merten, Laser-ablation absorption spectroscopy: reviewing an uncommon hyphenation, Spectrochim. Acta B At. Spectrosc. 189 (2022), 106358.
- [17] S.S. Harilal, B.E. Brumfield, N.L. LaHaye, K.C. Hartig, M.C. Phillips, Optical spectroscopy of laser-produced plasmas for standoff isotopic analysis, Appl. Phys. Rev. 5 (2018), 021301.
- [18] P.J. Skrodzki, N.P. Shah, N. Taylor, K.C. Hartig, N.L. LaHaye, B.E. Brumfield, I. Jovanovic, M.C. Phillips, S.S. Harilal, Significance of ambient conditions in uranium absorption and emission features of laser ablation plasmas, Spectrochim. Acta B At. Spectrosc. 125 (2016) 112–119.
- [19] A. El-Astal, T. Morrow, W. Graham, D.G. Walmsley, The role of gas-phase oxidation and combination during laser deposition of YBa2Cu3O7-x in ambient oxygen, Supercond. Sci. Technol. 8 (1995) 529.
- [20] H.F. Sakeek, T. Morrow, W.G. Graham, D.G. Walmsley, Optical absorption spectroscopy study of the role of plasma chemistry in YBa2Cu3O7 pulsed laser deposition, Appl. Phys. Lett. 59 (1991) 3631–3633.
- [21] T. Morrow, H.F. Sakeek, A. El Astal, W.G. Graham, D.G. Walmsley, Absorption and emission spectra of the YBCO laser plume, J. Supercond. 7 (1994) 823–828.

- [22] J. Merten, B. Johnson, Laser continuum source atomic absorption spectroscopy: measuring the ground state with nanosecond resolution in laser-induced plasmas, Spectrochim. Acta B At. Spectrosc. 139 (2018) 38–43.
- [23] A. Kramida, Y. Ralchenko, J. Reader, N.A. Team, NIST Atomic Spectra Database (Version 5.9), National Institute of Standards and Technology, Gaithersburg, MD, 2021.
- [24] P. Hannaford, R. Lowe, N. Grevesse, E. Biemont, W. Whaling, Oscillator strengths for YI and Y II and the solar abundance of yttrium, Astrophys. J. 261 (1982) 736–746.
- [25] X. Shang, Q. Wang, Y. Tian, C. Wang, Z. Dai, Radiative lifetimes, branching fractions, transition probabilities and oscillator strengths of some levels for neutral yttrium, J. Phys. B 48 (2015), 085001.
- [26] R.R.D. Weeks, M.C. Phillips, Y. Zhang, S.S. Harilal, R.J. Jones, Measurement of neutral gadolinium oscillator strengths using dual-comb absorption spectroscopy in laser-produced plasmas, Spectrochim. Acta B At. Spectrosc. 181 (2021), 106199.
- [27] A. Thorne, U. Litzén, S. Johansson, Spectrophysics: Principles and Applications, Springer Science & Business Media, 1999.
- [28] R.F. Wood, J.N. Leboeuf, D.B. Geohegan, A.A. Puretzky, K.R. Chen, Dynamics of plume propagation and splitting during pulsed-laser ablation of Si in he and Ar, Phys. Rev. B 58 (1998) 1533–1543.
- [29] J.A. Aguilera, C. Aragón, Characterization of a laser-induced plasma by spatially resolved spectroscopy of neutral atom and ion emissions: comparison of local and spatially integrated measurements, Spectrochim. Acta B At. Spectrosc. 59 (2004) 1861–1876.
- [30] C. Aragón, F. Peñalba, J.A. Aguilera, Spatial characterization of laser-induced plasmas: distributions of neutral atom and ion densities, Appl. Phys. A Mater. Sci. Process. 79 (2004) 1145–1148.
- [31] Y. Iida, Effects of atmosphere on laser vaporization and excitation processes of solid samples, Spectrochim. Acta B At. Spectrosc. 45 (1990) 1353–1367.
- [32] J.A. Merten, B.W. Smith, N. Omenetto, Local thermodynamic equilibrium considerations in powerchip laser-induced plasmas, Spectrochim. Acta B At. Spectrosc. 83-84 (2013) 50–55.
- [33] J.-F.Y. Gravel, D. Boudreau, Study by focused shadowgraphy of the effect of laser irradiance on laser-induced plasma formation and ablation rate in various gases, Spectrochim. Acta B At. Spectrosc. 64 (2009) 56–66.
- [34] D. Diaz, D.W. Hahn, Plasma chemistry produced during laser ablation of graphite in air, argon, helium and nitrogen, Spectrochim. Acta B At. Spectrosc. 166 (2020), 105800.
- [35] J.A. Merten, E. Ewusi-Annan, B.W. Smith, N. Omenetto, Optimizing gated detection in high-jitter kilohertz powerchip laser-induced breakdown spectroscopy. J. Anal. At. Spectrom. 29 (2014) 571–577.
- [36] M. Gaft, L. Nagli, I. Gornushkin, Y. Groisman, Doubly ionized ion emission in laserinduced breakdown spectroscopy in air, Anal. Bioanal. Chem. 400 (2011) 3229–3237.
- [37] R.T. Rhoades, R.R.D. Weeks, S.E. Erickson, C. Lecaplain, S.S. Harilal, M.C. Phillips, R. Jason Jones, Dual-comb absorption spectroscopy of molecular GeO in a laserproduced plasma, Opt. Lett. 47 (2022) 2502–2505.
- [38] A. De Giacomo, J. Hermann, Laser-induced plasma emission: from atomic to molecular spectra, J. Phys. D 50 (2017), 183002.